

Improvement of the redox stability of dithieno[3,2-b:2',3'-d]thiophene derivatives by using bulky substituents

Shinjiro Okada*, Kenji Yamada

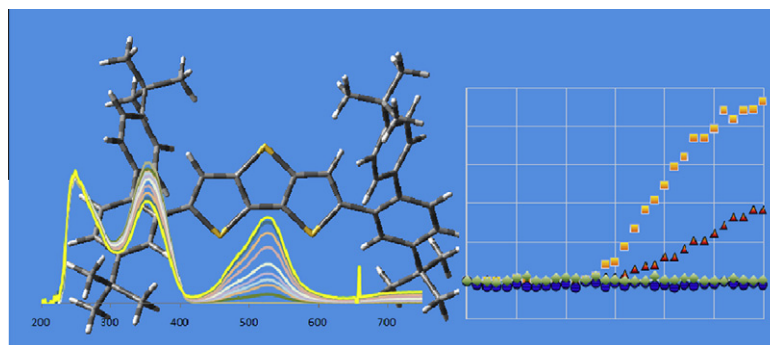
Nanomaterials Technology Development Center, Canon. Inc., 3-30-2 Shimomaruko, Ohtaku, Tokyo, Japan

HIGHLIGHTS

- ▶ Highly redox stable compounds were obtained using core-cage system.
- ▶ Bulky substituents on 2, 6 position of DTT revealed excellent redox stability.
- ▶ A large size substituent is more effective than a small size substituent.
- ▶ The core-cage system support electrochromicity and long stability at the same time.
- ▶ The photophysical and electrochemical properties were studied using various cages.

GRAPHICAL ABSTRACT

Substituent effects of dithieno[3,2-b:2',3'-d]thiophene (DTT) derivatives using bulky phenyl substitutions on its 2, 6 position were investigated. Dihedral angle between planes of the DTT and the phenyl affects strongly on photochemical and electrochemical properties. Especially, the molecule which has the DTT enfolded by the bulky substituent will be improved a long-term redox stability.



ARTICLE INFO

Article history:

Received 23 October 2012
 Received in revised form 30 December 2012
 Accepted 2 January 2013
 Available online 16 January 2013

Keywords:

Substituent
 Radical
 Cation
 Stability
 Electrochromic
 Redox

ABSTRACT

With the goal of improving the long term redox stability of dithieno[3,2-b:2',3'-d]thiophene (DTT), we synthesized derivatives with differently sized substituents. It is well known that substituents in the 2, 6 positions of DTT are active in this respect. We provide in this article more insight into mechanism. The present study provides the first support for a size effect. Large size substituents in the 2, 6 positions of the DTT are more effective than small size substituents. In these compounds, the DTT acts as a core of a molecule where the HOMO is located and the substituents work as a cage to protect the core from various attacks from the outside. This core-cage system is not only effective to prevent polymerization but also to increase the long term redox stability. The compounds with large size substituents, such as (1,1':3',1''-terphenyl)-2-yl and 4,4'-di-tert-butyl-(1,1'-biphenyl)-2-yl, showed excellent long term redox stability. The oxidation potential was maintained during repeated oxidation up to 17,000 and 20,000 times, respectively. The compounds with small size substituents, such as phenyl and mesityl, showed 1/10 or less of this durability. We show the substituent effects on repeated oxidation by investigating the electrochemical and photophysical properties.

© 2013 Elsevier B.V. All rights reserved.

1. Introduction

Organic materials which show electrochromicity involving conductive polymer and small organic molecule have been the subject of extensive studies for the past four decades. Especially, much

* Corresponding author. Tel.: +81 3 3758 2111; fax: +81 3 3757 3019.
 E-mail address: okada.shinjiro@canon.co.jp (S. Okada).

attention was paid to the fields of smart windows and paper like displays. However, redox stability was the most serious problem that needed to be overcome. If the materials could be made to exhibit long term redox stability during repeated switching of oxidation state, and had high transparency in the uncolored state, organic materials could become widely used in electrochromic devices.

The most commonly studied organic materials are viologen derivatives and polythiophene. Although, many electrochromic materials have been investigated with extensive research effort, there still remains the problem of their poor redox stability during frequent switching. In case of organic materials, the reaction process of electrochromism that consists of oxidation and reduction has been accompanied essentially by a generation of radical cation species and their extinction. Instability of oligothiophene radical cations has already been reported. The electrochemical response of terthiophene was degraded rapidly due to polymerization. However, introduction of blocking methyl substituents to the terminal α -positions of terthiophene was successful in increasing the stability of the radical cation and therefore reversible redox reaction could be achieved [1,2]. There was a report regarding the electrochemical stability of fused oligothiophene that have silyl groups at the terminal positions [3]. In the report, the fused oligothiophenes end capped by silyl groups showed reversible oxidation waves, indicative of the significant stability of the produced radical cation species in rigid ladder skeletons such as tetrathienoacene, hexathienoacene and octathienoacene. There were many reports concerning thiophene [4–11] and dithieno[3,2-*b*:2',3'-*d*]thiophene (DTT) derivatives [12–16]. A series of oligothiophenes surrounded by bicycle [2,2,2] octane was also reported [17,18]. Another paper pointed out that the intrinsic reactivity of oligomer radicals decreases rapidly as their conjugation length increases [19]. From this viewpoint, many kinds of conductive polymers have a great advantage in the radical cation stability owing to a long conjugation length in a long chain. Over the last two decades, better performance of electrochromic organic materials using conductive polymer has been reported [20–25].

A long conjugation length of the conductive polymer, which is at the root of electroconductivity, consequently, induces delocalization of hole and unpaired electron in the oxidative state. The delocalization increases the chemical stability of the oxidative molecule, but at the same time the neutral absorption band shifts to the visible range due to the long conjugation length, which leads to narrower band gap of the conductive polymer. Therefore, if we need high transparency of electrochromic materials in the neutral state, it is difficult to use conductive polymers. On the other hand, small molecule electrochromic materials have a great advantage to obtain high transmission in the neutral state, because it is possible to design a molecular structure that does not have an optical absorption in the visible wavelength range in the neutral state. However, there is no space for delocalization of hole and unpaired electron. Hence, the stability of cation radical species of small molecules is worse than that of the conductive polymer. Small molecule materials using the viologen skeleton were investigated energetically mainly in the 1970s. Viologen derivatives in the same way have a short conjugation length [26–30]. Additionally, viologen derivatives in many cases form insoluble film adhering to the electrode surface during a one electron reduction, which is unfavorable because it is a causal factor of degradation [31].

In this paper, we suggest that the redox stability can be improved by locking the DTT core in a "cage structure". The cage structure is intended to protect the radical cation, which forms the core of the molecules in oxidation state, from nucleophilic and/or electrophilic attacks in these oxidized molecules. The cage structure using large size substituents on 2, 6 positions of the DTT will be shown to be more effective than the cage structure

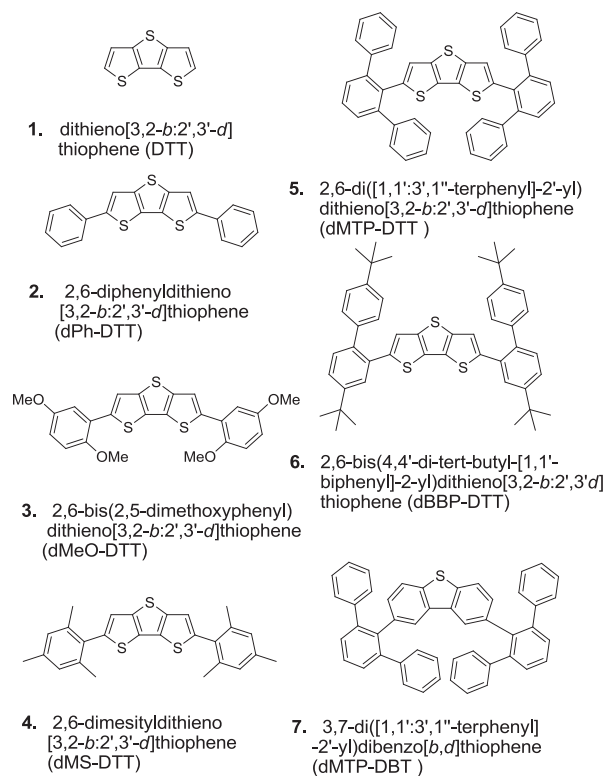
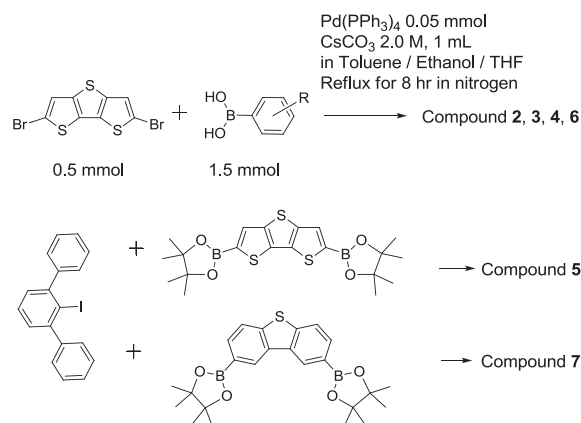


Fig. 1. Molecular structures of DTT derivatives and dMTP-DBT.



Scheme 1. Synthesis of compounds 2–7.

using small size substituents to stabilize the radical cation. We report synthesis, photophysical and electrochemical properties of materials based on the DTT skeleton. We address the goal of developing novel electrochromic materials having the cage structure based on DTT derivatives.

2. Experimental section

2.1. Synthesis

2.1.1. General

The outline of our synthetic routes to the 6 compounds listed in Fig. 1 is shown in Scheme 1. They were synthesized by Suzuki–Miyaura coupling of 2,6-dibromodithieno[3,2-*b*:2',3'-*d*]thiophene each with the corresponding boronic acid. Compounds 5 and 7 in Fig. 1 were also synthesized by Suzuki–Miyaura coupling of 3,7-bis(4,4,5,5-tetramethyl-1,3,2-dioxaborolan-2-yl)dibenzo [b,d]

thiophene and 2,6-bis(4,4,5,5-tetramethyl-1,3,2-dioxaborolan-2-yl)dithieno[3,2-*b*:2',3'-*d*] thiophene with 2'-iodo-1,1':3',1''-terphenyl, respectively. The typical procedure is following. A mixture of 2,6-dibromo-dithieno[3,2-*b*:2',3'-*d*]thiophene (174.0 mg, 0.5 mmol), boronic acid of counterpart (1.5 mmol), tetrakis (triphenylphosphine) palladium (81.5 mg, 0.08 mmol) and Cs₂CO₃ (2.0 mL, 2.0 M in aqueous) in 8 mL solvent of toluene: THF = 1:1 was stirred at reflux temperature for 8 h. All reactions were carried out under nitrogen atmosphere with anhydrous solvents. The mixture was poured into water (30 mL) and extracted with CH₂Cl₂ (20 mL × 3). The combined extract was washed with brine (40 mL), dried (Na₂SO₄), and concentrated in vacuo. Column chromatography on silica gel eluted with CHCl₃:toluene = 1:1. All compounds were characterized by ¹H and ¹³C NMR and mass spectroscopy.

Dithieno[3,2-*b*:2',3'-*d*]thiophene (DTT), 1:
ALDRICH, CAS: 3593-75-7

2,6-diphenyldithieno[3,2-*b*:2',3'-*d*]thiophene(dPh-DTT), 2:
[12,13];
¹H NMR (CDCl₃, 600 MHz), δ: (ppm) = 7.66 (d, 4H), 7.52 (s, 2H), 7.43 (t, 4H), 7.33 (t, 2H);
¹³C NMR (CDCl₃, 150 MHz), δ: (ppm) = 145.46, 142.04, 134.86, 130.65, 129.44, 128.25, 126.05, 116.92;
MS (ESI) m/z: (M⁺), (found) 348.0103, (Calc.) 348.0101;

2,6-bis(2,5-dimethoxyphenyl)dithieno[3,2-*b*:2',3'-*d*]thiophene (dMeO-DTT), 3:
¹H NMR (CDCl₃, 600 MHz), δ: (ppm) = 7.74 (s, 2H), 7.24 (d, 2H), 6.95 (d, 2H), 6.84 (dd, 2H), 3.94 (s, 6H), 3.84 (s, 6H);
¹³C NMR (CDCl₃, 150 MHz), δ: (ppm) = 154.19, 150.56, 141.48, 140.50, 131.80, 124.56, 119.47, 113.93, 113.90, 113.61, 56.76, 56.20;
MS (ESI) m/z: (M⁺), (found) 468.0489, (Calc.) 468.0524;

2,6-dimesityldithieno[3,2-*b*:2',3'-*d*]thiophene (dMS-DTT), 4:
¹H NMR (CDCl₃, 600 MHz), δ: (ppm) = 7.02 (s, 2H), 6.98 (s, 4H), 2.35 (s, 6H), 2.21 (s, 12H);
¹³C NMR (CDCl₃, 150 MHz), δ: (ppm) = 142.37, 140.38, 138.92, 138.84, 131.55, 131.23, 128.53, 120.36, 21.49, 21.11;
MS (ESI) m/z: (M⁺), (found) 432.1071, (Calc.) 432.1040;

2,6-di([1,1':3',1''-terphenyl]-2'-yl)dithieno[3,2-*b*:2',3'-*d*]thiophene (dMTP-DTT), 5:
¹H NMR (CDCl₃, 600 MHz), δ: (ppm) = 7.49 (dt, 2H), 7.41 (d, 4H), 7.21 (br, 20H), 6.50 (s, 2H);
¹³C NMR (CDCl₃, 150 MHz), δ: (ppm) = 143.63, 141.94, 141.47, 139.63, 131.93, 131.66, 130.20, 129.73, 128.68, 128.22, 127.05, 123.21;
MS (ESI) m/z: (M⁺), (found) 652.1412, (Calc.) 652.1353;

2,6-bis(4,4'-di-tert-butyl-[1,1'-biphenyl]-2-yl)dithieno[3,2-*b*:2',3'-*d*]thiophene(dBBP-DTT), 6:
¹H NMR (CDCl₃, 600 MHz), δ: (ppm) = 7.56 (d, 2H), 7.43 (dd, 2H), 7.33 (d, 2H), 7.30 (d, 4H), 7.21 (d, 4H), 6.81 (s, 2H), 1.39 (s, 18H), 1.31 (s, 18H);

¹³C NMR (CDCl₃, 150 MHz), δ: (ppm) = 150.77, 150.26, 144.98, 140.70, 138.35, 138.29, 132.99, 131.31, 131.14, 129.60, 128.09, 125.62, 125.45, 120.55, 34.94, 34.87, 31.73, 31.68;

MS (ESI) m/z: (M⁺), (found) 724.3207, (Calc.) 724.3231;
3,7-di([1,1':3',1''-terphenyl]-2'-yl)dibenzo[*b*,*d*] thiophene (dMTP-DBT), 7:

¹H NMR (THF-*d*₈, 600 MHz), δ: (ppm) = 7.48 (dd, 2H), 7.40 (d, 4H), 7.36–7.38 (m, 4H), 7.02–7.08 (m, 20H), 6.88 (dd, 2H);

¹³C NMR (THF-*d*₈, 150 MHz), δ: (ppm) = 140.82, 140.47, 137.3, 135.72, 134.48, 133.15, 128.65, 128.14, 127.85, 125.83, 125.62, 124.41, 123.01, 119.55;

MS (ESI) m/z: (M⁺), (found) 640.2253, (Calc.) 640.2225.

2.2. Instrumentation

¹H NMR (600 MHz) and ¹³C NMR (150 MHz) spectra were recorded on a Bruker model AVANCE-600 NMR spectrometer. The mass spectrometric analysis was carried out in positive ion mode on a Waters MICROMASS, Q-TOF Ultima spectrometer equipped with an ESI source. The capillary and cone voltages were set at 3000 and 80 V, respectively. The desolvation and source temperatures were set to 150 and 80 °C, respectively. The cone gas flow and desolvation gas flow were 50 and 600 L/h, respectively. Electrochemical measurements were performed using a three electrodes cell with a platinum wire as a counter electrode, an Ag/Ag⁺ reference electrode in 0.1 M tetra butyl ammonium perchlorate (n-Bu₄ NClO₄) in CH₂Cl₂ or CH₂Cl–CH₂Cl electrolyte and a glassy carbon as a working electrode. All potentials are recorded against an Ag/Ag⁺ reference. A Solatron electrochemical interface model SI 1287 was used under control of Corrware software. The electrolyte solution was purged in 10 min with nitrogen before electrochemical measurement commenced. UV–visible absorption spectra were measured using a JASCO V-560 spectrometer. Absorption spectra in oxidized state were obtained using an Ocean Optics USB4000-UV–vis spectrometer with a 1 mm thin layer quartz cell with three electrodes and a Solatron electrochemical interface model SI 1287 as voltage source. Photophysical measurements in the neutral state were performed with CH₂Cl₂ solution. Ab-initio calculation of the electronic state of the compounds were performed to obtain the minimum energy structure in the neutral and oxidized state using the Gaussian-03 software package (Gaussian Inc.) with density functional theory b3lyp calculation and bases set 6-31G* [32].

3. Results and discussion

3.1. Electrochemical properties

The electrochemical properties of the compounds shown in Fig. 1 were investigated. To examine the redox behavior of newly synthesized compounds **3–6**, cyclic voltammetric (CV) measurements were performed in methylene chloride at room

Table 1
Electrochemical data^a for DTT derivatives and dibenzothiophene derivative.

Compounds	<i>E</i> _{ox} (V)	<i>E</i> _{red} (V)	<i>E</i> _{ox1/2} (V)	d <i>E</i> (mV)	HOMO ^b (eV)	θ ^c (°)
1 DTT	1.12	–	Irreversible		–5.58	
2 dPh-DTT	0.85	0.79	0.82	63	–5.17	28
3 dMeO-DTT	0.53	0.42	0.47	117	–4.95	28
4 dMS-DTT	1.01	0.94	0.98	70	–5.36	90
5 dMTP-DTT	0.84	0.79	0.81	59	–5.12	60
6 dBBP-DTT	0.85	0.78	0.82	72	–5.01	41
7 dMTP-DBT	1.39	–	Irreversible		–5.55	61

^a Scan rate of cyclic voltammetry was 25 mV/s. The counter electrode was Pt wire and the reference was Ag/Ag⁺ with a glassy carbon as a working electrode, all potentials were referenced versus the Ag/Ag⁺ in CH₂Cl₂ with an electrolyte 0.1 M TBAP.

^b HOMO is calculated by Gaussian-03.

^c Dihedral angle is calculated by Gaussian-03.

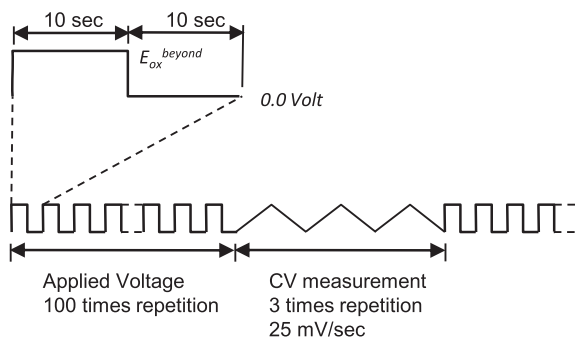


Fig. 2. Voltage application sequence to measure long term redox stability.

temperature. The resulting oxidation and reduction potentials are summarized in Table 1 together with those for compound 1 (DTT), known DTT derivatives compound 2 and compound 7 for comparison. The electrochemical oxidation and reduction reaction of compounds 2–6 is reversible, so that the CVs show comparable, symmetrical anodic and cathodic waves. While compounds 2–6 exhibit reversible first oxidation waves, compound 1 (DTT) shows irreversible redox waves due to easy polymerization [19,33–35]. In this experiment, electro polymerization occurred on the working electrode as soon as potential was applied to the electrode. Consequently, the working electrode was coated with black deposits. It was necessary to protect the 2, 6 positions of the DTT core using some kind of substituent to obtain redox reversibility even in for a few cycles only.

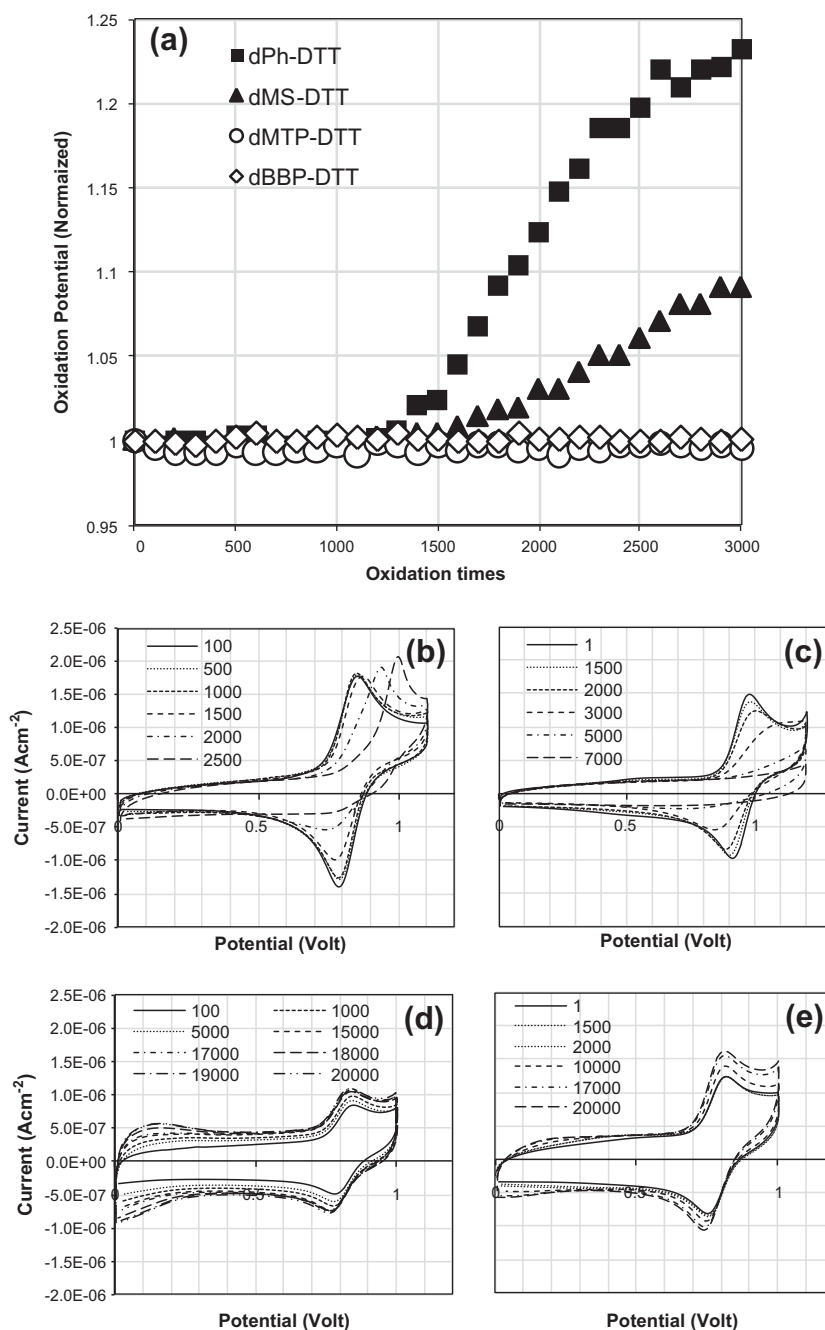


Fig. 3. Variation of oxidation potential during repetitive oxidation. (a) oxidation peak shift during repetition (b–e) are cyclic voltammograms of (b) dPh-DTT, (c) dMS-DTT, (d) dMTP-DTT and (e) dBBP-DTT 0.1 mM in methylene chloride (b and c) in ethylene chloride (d and e) with 0.1 M TBAP, sweep rate was 25 mV/s.

The oxidation potential is affected by the conjugation length which is linked to the energy of the HOMO. Now we defined a dihedral angle as the calculated angle between the DTT plane and the phenyl plane of the substituent as shown in Table 1. The dihedral angles of compounds 2–6 should have much effect on each oxidation potential. As expected, compound 4 that has a substituent with large steric hindrance exhibit the higher oxidation potential ($E_{ox1/2}$) compared to the other compounds in this study. This compound 4 reveals relatively short conjugation length that is attributable to the large dihedral angle. However, compounds 2, 5 and 6 have similar $E_{ox1/2}$ in spite of different dihedral angles among them. Compound 3 shows lower oxidation potential than other compounds. It might be derived from longer conjugation length due to lower dihedral angle and strong electron donation owing to methoxy substituents of phenyl attachment to DTT. Experimental results of oxidation potential show a nearly proportionate relationship to the calculated energy of the HOMO as listed in Table 1. From these results, it seems that the difference of oxidation potentials among these compounds is connected with the structural configuration of the molecules to some degree. We picked four compounds, which had redox reversibility for a short period, to investigate the long term redox stability.

3.2. Long term redox stability

To investigate the long term stability during switching between oxidation and neutral state, the electrochemical measurement was reported by applying rectangular voltage pulses to compounds 2 (dPh-DTT), 4 (dMS-DTT), 5 (dMTP-DTT) and 6 (dBBP-DTT) in the three electrodes cell as shown in Fig. 2. Rectangular voltage pulses consisted of two 10 s pulses. The voltage of the first pulse was E_{ox}^{beyond} and that of the second pulse was 0.0 V, where E_{ox}^{beyond} is the potential which is 0.1 V higher than the potential for first oxidation peak for each compound. The CV measurement was carried out three times after every 100 pulses to the cell. The three electrodes cell was composed of a platinum wire as a counter electrode, Ag/Ag⁺ reference electrode and a glassy carbon electrode as a working electrode in 0.1 M tetra butyl ammonium perchlorate (*n*-Bu₄NClO₄) and 0.1 mM compound as an object to be measured in CH₂Cl₂ or C₂H₄Cl₂ electrolyte solution. All potentials are reported against an Ag/Ag⁺ reference.

Fig. 3a shows oxidation peak shifts of compounds in long term redox repetition between oxidation and neutral state. Fig. 3b–e show the CV waveforms of compounds 2, 4, 5 and 6. Measurement of long term redox stability was done with 1,2-dichloroethane for solvent to avoid volatilization. However, the volatilization occurred at repetition in excess of 10,000 times, as shown in Fig. 3d and e

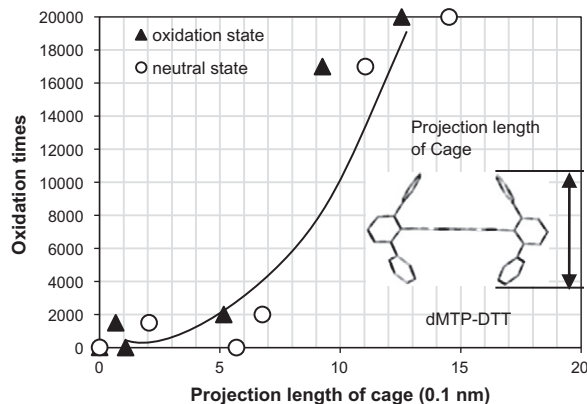


Fig. 4. Lifetime under oxidation of DTT derivatives with different cage structure. Projection length of cage was obtained by calculation with Gaussian-03.

Table 2
Photophysical data for compounds listed Fig. 1.

Compounds	Absorption peak (nm)		ϵ^b ($M^{-1} cm^{-1}$)
	Neutral state	Oxidation state ^a	
1 DTT	282 ^s , 292	386	37,500
2 dPh-DTT	370	474, 526	40,780
3 dMeO-DTT	319, 386, 408 ^s	578	46,255
4 dMS-DTT	309, 318	350, 429, 495	18,559
5 dMTP-DTT	243, 278 ^s , 348	479	20,350
6 dBBP-DTT	357	519	27,919
7 dMTP-DBT	243, 292 ^s , 324 ^s		13,631

^s Shoulder absorption peak.

^a Maximum absorption peak at oxidation state.

^b Molar absorption coefficient " ϵ " was measured at first absorption peak in neutral state.

and the CV current increased due to condensation of solution. Oxidation peak potential of dPh-DTT 2 shifted to 5% higher potential at around 1500 repetitions. In case of dMS-DTT 4, 5% higher shift of potential peak occurred at 2500 repetitions as shown in Fig. 3a. The peak shift of dMTP-DTT 5 did not occur after 3000 times and even after 17,000 times. Furthermore, the peak shift of dBBP-DTT 6 did not occur after 20,000 repetitions. The oxidation peaks of dMTP-DTT 5 and dBBP-DTT 6 remained clearly distinguishable after 17,000 and 20,000 cycles without obvious generation of reaction product accompanied with new oxidation peak generation. This result shows that dMTP-DTT 5 and dBBP-DTT 6 have excellent stability regarding oxidation peak shift during long term redox repetition more than that of dPh-DTT 2 and dMS-DTT 4. Compounds 2, 5 and 6 have similar oxidation potential potential $E_{ox1/2}$, but a different cage structure and different long term redox stability.

Lastly, we show the long term redox stability of compounds using different cage structures in Fig. 4. Lifetime is taken from 20% decrease of oxidation peak current or a peak shift of more than 5%. To represent the size effect of the cage structure, we try to use the projection length of the cage structure. The projection length is defined as orthogonal projection of cage size to the orthogonal plane of the DTT plane using DFT calculation as shown in inset in Fig. 4. It is likely that the long term redox stability has a high correlation with the oxidized molecular structure of the compound as well as the molecular structure in neutral state. In Fig. 4, the plots of filled triangles show projection length of the oxidation state and the plots of opened circles show neutral state projection lengths, both of which are calculated from the minimum energy structure obtained from the DFT calculation program. As shown in Fig. 4, longer projection length of oxidation and neutral state corresponds to higher long term redox stability. Consequently, the compounds 5, 6 having longer projection length show excellent durability. The durability times for retaining the oxidation potential of the initial value, of dPh-DTT 3, dMS-DTT 4, dMTP-DTT 5 and dBBP-DTT 6 as shown in Fig. 4 are 1500, 2000, 17,000 and over 20,000. The 20,000 times is only an upper limitation of this measurement due to volatilization of solvent of this measurement. From these results, it is clear that the large size substituent, which was used for the cage structure, is quite effective in improving the long term redox stability.

3.3. The speculations of underlying cause about size effect

We suggest two explanations for the improvement of the long term redox stability using large size substituents. The first is a reduction of the intermolecular interaction due to the large size substituent suggested by the photophysical properties. The photophysical properties of the compounds shown in Fig. 1 were investigated using UV–vis spectroscopy. The UV–vis spectroelectrochemical oxidation

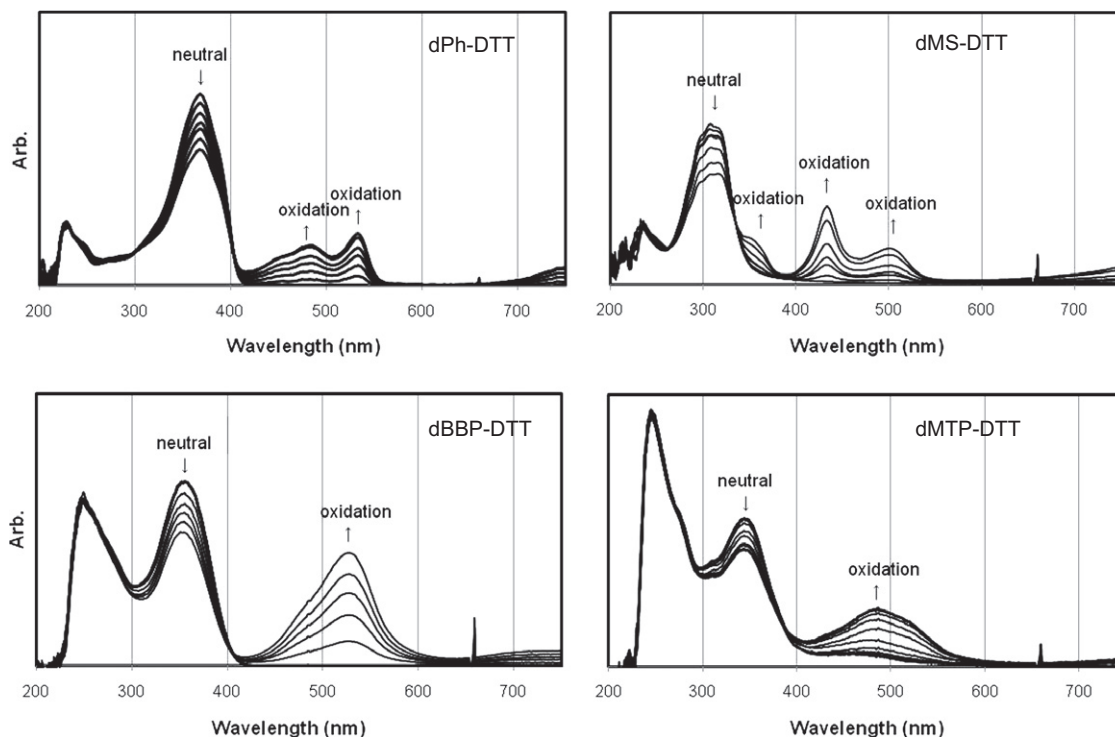


Fig. 5. Spectroelectrochemical oxidation of dPh-DTT, dMS-DTT, dMTP-DTT and dBBP-DTT 0.1 mM in methylene chloride with 0.1 M TBAP.

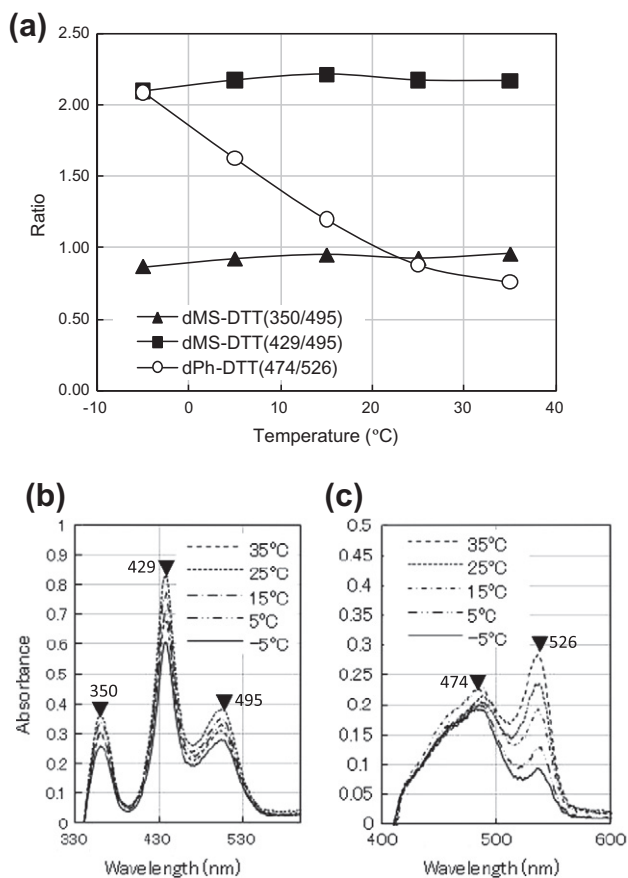


Fig. 6. (a) Visible band absorption ratio of dMS-DTT and dPh-DTT 1 mM in methylene chloride with 0.1 M TBAP. Set of optical spectra of the first oxidation state of (b) dMS-DTT and (c) dPh-DTT at different temperatures.

of the compounds was carried out in 1 mm thin layer quartz cell with methylene chloride solvent as described in experimental section. The absorption peaks in both neutral and oxidation states of seven compounds in Fig. 1 in methylene chloride are listed in Table 2. Though the compounds, dPh-DTT **3** and dMS-DTT **4**, had multiple absorption peaks in the visible range at oxidation state, dMTP-DTT **5** and dBBP-DTT **6** had only a single absorption peak as shown in Fig. 5. It is well known that the cation radicals form π dimers in association with the shift in the π - π^* absorption band [2] and the formation of π dimers is temperature dependent [11]. Fig. 6a shows the temperature dependence of the intensity ratio in the oxidation process between 474 nm and 526 nm for dPh-DTT **3** and between 350 nm, 429 nm and 495 nm for dMS-DTT **4**. Fig. 6b and c shows the spectral change of dPh-DTT **3** and dMS-DTT **4** depending on the temperature. The ratio of peak intensity of dPh-DTT **3** was dependent on the temperature as shown in Fig. 6. Hence, the multiple peaks of dPh-DTT **3** were supposed to be induced by π dimer formation [11]. However, ratio of peak intensity between the multiple peaks of dMS-DTT **4** remained unaltered by temperature change as shown in Fig. 6a. The result means that the multiple absorption peaks of dMS-DTT **4** are intrinsic cation peaks. From these results, it is probable that the large size substituents on 2, 6 positions of DTT core work to prevent π dimer formation. Therefore, it seems that the larger size substituent will weaken intermolecular interactions. This finding is consistent to the result of superior long term redox stability of compounds, dMTP-DTT **5** and dBBP-DTT **6**.

Another explanation of the results is a localization of the HOMO to the core portion. Fig. 7 shows the HOMO surface of compounds listed in Fig. 1. It seems that dPh-DTT **3** is easily attacked from outwards, because dPh-DTT **3** has the HOMO not only in the DTT but also in the cage. However, it seems that the compounds of dMS-DTT **4**, dMTP-DTT **5** and dBBP-DTT **6** are protected against attack from outwards owing to localizing the HOMO to interior of the molecule using cage structure as shown in Fig. 7. Compounds **4** and **5**, which have a relatively large dihedral angle, have large steric hindrance at both ortho positions of the phenyl attached to the

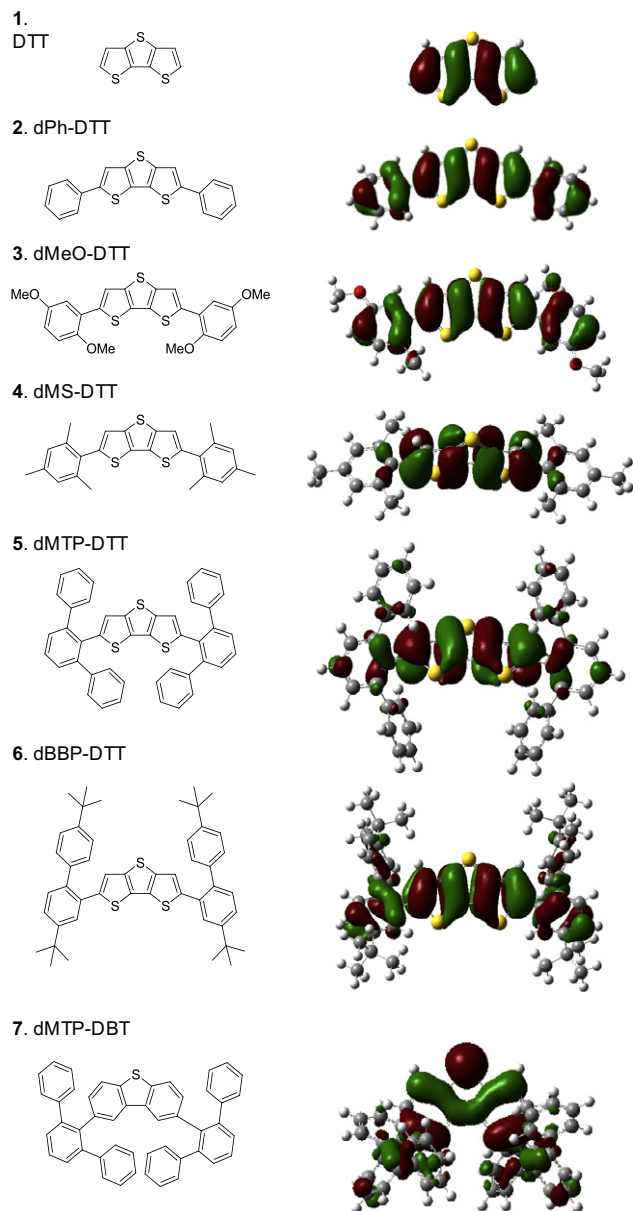


Fig. 7. Distribution of HOMO on neutral state calculated by Gaussian-03. Dihedral angle between cage and core affected to distribution of HOMO in the neutral state. Large dihedral angle localized HOMO to the core due to orthogonal molecular orbital between them. Compounds **4**, **5** and **6** have mainly localized HOMO to the core. (Be reproduced in color on the Web (free of charge) and in black-and-white in print).

DTT core. Oxidation peak shift of dMS-DTT **4** is larger than that of dMTP-DTT **5** and dBBP-DTT **6**. This will be attributing to the length of cage structure of dMS-DTT **4**, which is shorter than dMTP-DTT **5** and dBBP-DTT **6**. It is likely that the length is insufficient to cover enough to prevent attack from outside. On the other hand, while compound **6** shows medium dihedral angle, it has a quite bulky structure. Therefore, large size substituents of dMTP-DTT **5** and dBBP-DTT **6** are expected to work as efficient cage to protect DTT core from attack. It is likely that the restriction of localization of HOMO to the core portion through use of a core-cage system is associated with the decrease of the reactivity of the corresponding radical cation, since the radical cation is generated in the HOMO by oxidation.

Though the dMTP-DBT **7** has the same substituent as cage as dMTP-DTT **5**, dMTP-DBT **7** showed inferior redox stability as shown in Table 1. In our understanding, the difference derives from

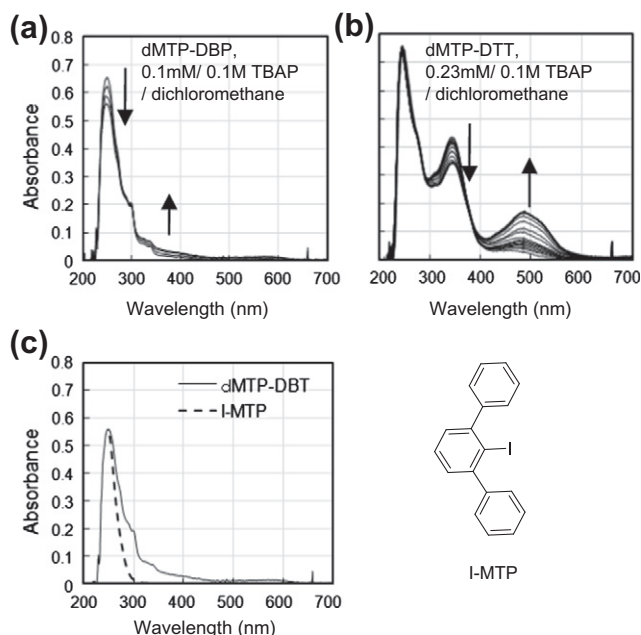


Fig. 8. Spectroelectrochemical data of dMTP-DBT, dMTP-DTT and I-MTP.

the different HOMO composition. dMTP-DTT **5** has two absorption peaks in the neutral state. During the oxidation progress of dMTP-DTT **5**, one neutral absorption peak of 348 nm diminished and a new cationic absorption peak of 480 nm appeared. However, another neutral absorption peak of 243 nm of dMTP-DTT **5** did not change any more as shown in Fig. 8b. Though compound dMTP-DBT **7** had a neutral absorption peak at 243 nm, the peak diminished during the oxidation process as shown in Fig. 8a. dMTP-DTT **5** and dMTP-DBT **7** have same cage structure and almost the same dihedral angle as seen in Table 1. However, core structures of these two compounds are different. dMTP-DTT **5** has DTT as a core. On the other hand dMTP-DBT **7** has dibenzothiophen (DBT) as a core. The DTT is an electron rich fused ring structure, richer than the DBT. dMTP-DBT **7** has a wider band gap and higher oxidation potential than dMTP-DTT **5** as listed in Tables 1 and 2. The neutral absorption peak of 243 nm of dMTP-DTT **5** and 243 nm of dMTP-DBT **7** belongs to the cage part absorption that is commonly found. It is obvious by making a comparison of absorption peaks between iodine meta terphenyl and dMTP-DBT **7** as shown in Fig. 8 (c). It is important that in the case of dMTP-DBT **7**, the cage oxidized at a first oxidation potential, 1.39 V, while in the case of dMTP-DTT **5**, only the core oxidized at a first oxidation potential, 0.84 V, in the electrochemical oxidation process. The HOMO energy of the DTT and the DBT calculated by Gaussian 03/b3lyp/6-31G* were -5.58 eV and -5.80 eV, respectively. In fact, DTT oxidized at 1.12 V which was lower than the oxidation potential of dMTP-DBT **7**, 1.39 V. We acknowledge that dMTP-DBT **7** has a HOMO leaking to the outer shell because of low HOMO energy. Furthermore, the HOMO is expanded outwards due to the substitute positions of dMTP-DBT **7** as shown in Fig. 7. However, dMTP-DTT **5** has a HOMO mainly in the core portion because HOMO energy of DTT is higher than the orbital energy of the cage portion. These results explain that the compounds with the same cage structure but different core structure have different electrochemical properties as seen in Table 1.

4. Conclusions

The result of our experiments clearly shows that the DTT derivatives having large size substituents at 2, 6 positions have excellent

long term redox stability. Although the high reactivity of the 2, 6 positions of DTT due to high spin density is well known, we would like to focus attention to the size of substituents. It is notable that a large size substituent is more effective to stabilize the redox state than a small size substituent. It is likely that the large size cage structure protects the core in which the HOMO exists and prevents degradation. In other words, it is suggested that the reactivity of the radical cation would be reduced by use of the large size cage structure, therefore the long term redox stability of a small molecule increased in spite of a short conjugation length relative to conductive polymers.

The compounds with large size substituents such as 4,4'-di-tert-butyl-(1,1'-biphenyl)-2-yl and (1,1':3',1''-terphenyl)-2-yl show good electrochromicity and excellent long term redox stability of 17,000 times and over 20,000 times in repeated oxidation, respectively. Long term reversible behavior is a notable feature for the present core-cage system that promises the potential use as an electrochromic and electroconductive material in organic electronics. Further studies on the core-cage structural design of dithieno[3,2-b:2',3'-d]thiophene (DTT) derivatives as well as their application in organic electrochromic devices are now in progress in our group.

Appendix A. Supplementary material

Supplementary data associated with this article can be found, in the online version, at <http://dx.doi.org/10.1016/j.molstruc.2013.01.002>.

References

- [1] M.G. Hill, J.F. Penneau, B. Zinger, K.R. Mann, L.L. Miller, *Chem. Mater.* 4 (1992) 1106.
- [2] M.G. Hill, K.R. Mann, L.L. Miller, J.F. Penneau, *J. Am. Chem. Soc.* 114 (1992) 2728.
- [3] T. Okamoto, K. Kudoh, A. Wakamiya, S. Yamaguchi, *Chem. Eur. J.* 13 (2007) 548.
- [4] K. Takimiya, N. Niihara, T. Otsubo, *Synthesis* 10 (2005) 1589.
- [5] S. Zhang, Y. Guo, H. Xi, C. Di, J. Yu, K. Zheng, R. Liu, X. Zhan, Y. Liu, *Thin Solid Films* 517 (2009) 2968.
- [6] N. Metri, X. Sallenave, L. Beouch, C. Plesse, F. Goubard, C. Chevrot, *Tetrahedron Lett.* 51 (2010) 6673.
- [7] C. Kima, M. Chenb, Y. Chiangb, Y. Guob, J. Youna, H. Huang, Y. Liangb, Y. Linb, Y. Huangb, T. Hub, G. Leed, A. Facchetti, T.J. Marks, *Org. Electron.* 11 (2010) 801.
- [8] W. Schroth, E. Hintzsche, H. Jordan, T. Jende, R. Spitzner, I. Thondorf, *Tetrahedron* 53 (1997) 7509.
- [9] L. Wang, Q. Chen, G. Pan, L. Wan, S. Zhang, X. Zhan, B.H. Northrop, P.J. Stang, *J. Am. Chem. Soc.* 130 (2008) 13433.
- [10] W. Schroth, E. Hintzsche, M. Felicetti, R. Spitzner, J. Sieler, R. Kempe, *Angew. Chem. Int. Ed.* 33 (1994) 739.
- [11] B. Yina, C. Jianga, Y. Wanga, M. Laa, P. Liua, W. Deng, *Synth. Met.* 160 (2010) 432.
- [12] O.H. Omar, F. Babudri, G.M. Farinola, F. Naso, *Tetrahedron* 67 (2011) 486.
- [13] W. Porzio, S. Destri, U. Giovanella, M. Pasini, L. Marin, M.D. Iosip, M. Campione, *Thin Solid Films* 515 (2007) 7318.
- [14] P. Liu, X. Wang, Y. Zhang, X. Zhou, W. Deng, *Synth. Met.* 155 (2005) 565.
- [15] Y.M. Sun, Y.Q. Ma, Y.Q. Liu, Y.Y. Lin, Z.Y. Wang, Y. Wang, C.A. Di, K. Xiao, X.M. Chen, W.F. Qiu, B. Zhang, G. Yu, W.P. Hu, D.B. Zhu, *Adv. Funct. Mater.* 16 (2006) 426.
- [16] P. Baeuerle, U. Segelbacher, A. Maier, M. Mehring, *J. Am. Chem. Soc.* 115 (1993) 10217.
- [17] T. Nishinaga, A. Wakamiya, D. Yamazaki, K. Komatsu, *J. Am. Chem. Soc.* 126 (2004) 3163.
- [18] A. Wakamiya, D. Yamazaki, T. Nishinaga, T. Kitagawa, K. Komatsu, *J. Org. Chem.* 68 (2003) 8305.
- [19] Z. Xu, D. Fichou, G. Horowitz, F. Garnier, *J. Electroanal. Chem.* 267 (1989) 339.
- [20] A.L. Dyer, M.R. Craig, J.E. Babiary, K. Kiyak, J.R. Reynolds, *Macromolecules* 43 (2010) 4460.
- [21] P.M. Beaujuge, S. Ellinger, J.R. Reynolds, *Nat. Mater.* 7 (2008) 795.
- [22] G. Sonmez, H. Meng, Q. Zhang, F. Wudl, *Adv. Funct. Mater.* 13 (2003) 726.
- [23] B. Sankaran, J.R. Reynolds, *Macromolecules* 30 (1997) 2582.
- [24] M. Li, A. Patra, *Adv. Mater.* 21 (2009) 1707.
- [25] P.H. Aubert, A.A. Argun, A. Cirpan, D.B. Tanner, J.R. Reynolds, *Chem. Mater.* 16 (2004) 2386.
- [26] T. Kawata, M. Yamamoto, M. Yamana, M. Tajima, T. Nakano, *Jpn. J. Appl. Phys.* 14 (1975) 725.
- [27] C.J. Schoot, J.J. Ponjee, H.T. van Dam, R.A. van Doorn, P.T. Bolwijn, *Appl. Phys. Lett.* 23 (1973) 64.
- [28] M. Yamana, *Jpn. J. Appl. Phys.* 15 (1976) 2469.
- [29] J. Bruinink, P. van Zanten, *J. Electrochem. Soc.* 124 (1977) 1232.
- [30] D.J. Barclay, B.F. Dowden, A.C. Lowe, J.C. Wood, *Appl. Phys. Lett.* 42 (1983) 911.
- [31] R.J. Mortimer, *Chem. Soc. Rev.* 26 (1997) 147.
- [32] M.J. Frisch, G.W. Trucks, H.B. Schlegel, G.E. Scuseria, M.A. Rob, J.R. Cheeseman, J.A. Montgomery Jr., T. Vreven, K.N. Kudin, J.C. Burant, J.M. Millam, S.S. Iyengar, J. Tomasi, V. Barone, B. Mennucci, M. Cossi, G. Scalmani, N. Rega, G.A. Petersson, H. Nakatsuji, M. Hada, M. Ehara, K. Toyota, R. Fukuda, J. Hasegawa, M. Ishida, T. Nakajima, Y. Honda, O. Kitao, H. Nakai, M. Klene, X. Li, J.E. Knox, H.P. Hratchian, J.B. Cross, V. Bakken, C. Adamo, J. Jaramillo, R. Gomperts, R.E. Stratmann, O. Yazyev, A.J. Austin, R. Cammi, C. Pomelli, J.W. Ochterski, P.Y. Ayala, K. Morokuma, G.A. Voth, P. Salvador, J.J. Dannenberg, V.G. Zakrzewski, S. Dapprich, A.D. Daniels, M.C. Strain, O. Farkas, D.K. Malick, A.D. Rabuck, K. Raghavachari, J.B. Foresman, J.V. Ortiz, Q. Cui, A.G. Baboul, S. Clifford, J. Cioslowski, B.B. Stefanov, G. Liu, A. Liashenko, P. Piskorz, I. Komaromi, R.L. Martin, D.J. Fox, T. Keith, M.A. Al-Laham, C.Y. Peng, A. Nanayakkara, M. Challacombe, P.M.W. Gill, B. Johnson, W. Chen, M.W. Wong, C. Gonzalez, J.A. Pople, *Gaussian 03*, Gaussian, Inc., Wallingford, CT, 2003.
- [33] F. Garnier, G. Tourillon, M. Gizard, J.C. Dubois, *J. Electroanal. Chem.* 148 (1983) 299.
- [34] A. Smie, A. Synowczyk, J. Heinze, R. Alle, P. Tschuncky, G. Götz, P. Bäuerle, *J. Electroanal. Chem.* 452 (1998) 87.
- [35] P. Tschuncky, J. Heinze, *Synth. Met.* 55 (1993) 1603.